Materials Advances

ROYAL SOCIETY OF CHEMISTRY

PAPER

View Article Online
View Journal | View Issue

Check for updates

Cite this: *Mater. Adv.*, 2020, 1, 814

Synthesis, fluorescence property and cell imaging of a perylene diimide-based NIR fluorescent probe for hypochlorite with dual-emission fluorescence responses†

Huan-ren Cheng, *[a] Botao Qu,[b] Chen Qian,[a] Meng Xu*[c] and Ruiping Zhang*[b]

Received 25th March 2020,
Accepted 6th June 2020

DOI: 10.1039/d0ma00131g

rsc.li/materials-advances

In this study, for the first time, a novel near-infrared and ratiometric fluorescent probe was conveniently synthesized by reacting PDI-based salicylaldehyde with 2-(hydrazonomethyl)phenol. The probe was designed based on the intramolecular charge transfer (ICT) mechanism and the intramolecular electron transfer (IET) mechanism, which can be blocked by the hypochlorite and a larger conjugation is formed within the probe. Due to the turn-on fluorescence responses triggered by the PET and ICT processes after the ClO^- addition, the probe produces simultaneous emission peaks at 600 nm and 820 nm. In addition, the probe shows a rapid fluorescence response towards the ClO^- ions within 5 s, a low detection limit (0.8×10^{-7} M), intense color changes (from purple to light green), excellent selectivity, and reversibility. Importantly, cell imaging experiments show that the probe can identify endogenous ClO^- successfully.

Introduction

Fluorescent chemosensors because of their fast detection speed, high sensitivity and simple operation have been widely used in biological tracing, ion detection, environmental protection and other fields. Today, fluorescent chemosensors used as detection tools for toxic ions or small molecules are getting increasing attention. In recent years, a large number of fluorescent sensors for the detection of ions or small molecules have been reported.[1–5] Among these ions or small molecules, hypochlorite (ClO^-) as a reactive oxygen species plays an important role in our daily life. However, excessive hypochlorite easily causes a variety of diseases.[6–8] Therefore, it is necessary to develop fluorescent chemosensors for the real-time monitoring of hypochlorous acid/hypochlorite.

To date, numerous fluorescent probes for ClO^- have been reported.[9–25] Most of these fluorescence probes for ClO^- were a type of short wavelength response probes. Such probes have some prominent disadvantages, such as strong background effect, shallow imaging depth, and poor anti-infection ability. In order to overcome these defects, near-infrared ratiometric fluorescent probes were developed quickly.[26–30] Compared with the common fluorescent probes, near-infrared ratiometric fluorescent probes are overwhelming because of their unique advantages: deeper imaging depth, stronger anti-interference energy, and less tissue damage.

It is known that perylene diimide (PDI) derivatives as excellent fluorophores have been widely studied, most of them are designed based on the PET mechanism, and almost none are designed based on both the PET and ICT mechanism.[31–36] In this study, a new near-infrared ratiometric fluorescence probe, namely **PDI-SY**, was successfully designed and easily obtained by a direct condensation reaction between the PDI-based salicylaldehyde and 2-(hydrazonomethyl)phenol (Fig. 1). **PDI-SY** produces simultaneous emission peaks at 600 nm and 820 nm, when ClO^- is added. In addition, **PDI-SY** shows high sensitivity and selectivity in a fluorescence "turn-on" manner, the probe can efficiently monitor ClO^- with rapid fluorescence responses within 5 s, with a low detection limit (0.8×10^{-7} M) and intense color changes (from purple to light green). Further ^{1}H-NMR study also suggests that the PET and ICT mechanisms were involved after the addition of ClO^- ions. Moreover, the cell imaging experiments show that the probe can identify endogenous ClO^- successfully.

Results and discussion

Synthesis of the probe PDI-SY

The preparation of **PDI-SY** is shown in Scheme 1, the key intermediate compound **PDI-Y** was prepared *via* a simple electrophilic

[a] School of Chemical Engineering, Yangzhou Polytechnic Institute, Yangzhou 225127, China. E-mail: cheng_huanren@163.com
[b] School of Basic Medical Sciences, Shanxi Medical University, Taiyuan 030001, China. E-mail: zrp-7142@163.com
[c] Tongji Medical College, Huazhong University of Science and Technology, Wuhan 430022, China. E-mail: Xumeng@163.com

† Electronic supplementary information (ESI) available. See DOI: 10.1039/d0ma00131g

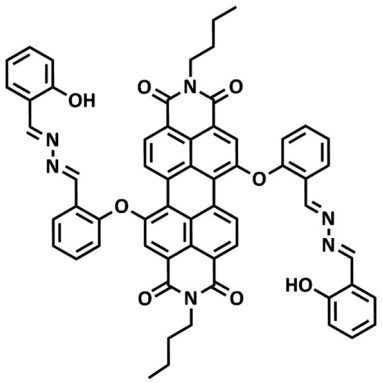

Fig. 1 Structure of the probe **PDI-SY**.

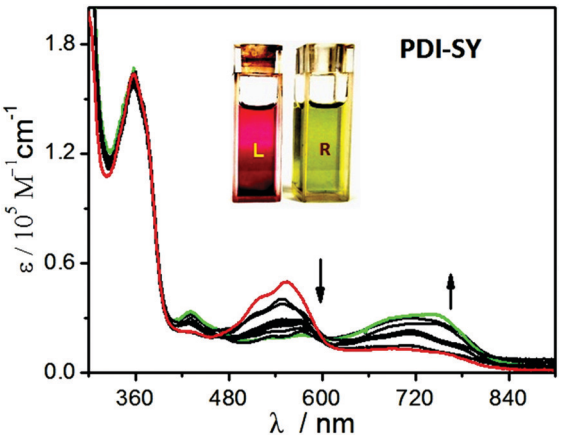

Fig. 2 Ratiometric absorption spectra of **PDI-SY** as a function of the ClO^- concentration, ([**PDI-SY**] = 2 μM, V_{THF/H_2O} = 1 : 3, pH = 7.4, PBS buffer). The inset picture shows the color change of **PDI-SY** upon the addition of ClO^-, L: **PDI-SY**, R: **PDI-SY** + ClO^-.

substitution reaction between **PDI-S** and salicylaldehyde, affording **PDI-Y** with 95% yield. All the intermediates and materials used in the synthesis process do not need to be further purified, the materials are cheap and readily available, which greatly reduce the synthesis cost of the probe **PDI-SY**. All the intermediates and the probe molecule **PDI-SY** were fully characterized *via* ^{1}H NMR, ^{13}C NMR, and high-resolution mass spectrometry (HRMS-MALDI-TOF); the detailed synthesis procedure of the **PDI-SY** has been discussed in the synthesis part.

Ratiometric absorption and dual emission of PDI-SY before and after reaction with ClO^-

The absorption and fluorescence emission properties of **PDI-SY** (2 μM) before and after the reaction with ClO^- were studied in an optimized mixture of the PBS buffer solution (pH 7.4). All the measurements were carried out in PBS buffer (pH 7.4). As shown in Fig. 2, **PDI-SY** exhibited maximum absorption peaks at around 354 nm and 556 nm without any other ions. Moreover, **PDI-SY** showed a weak emission at 520 nm, as shown in Fig. 3. However, upon the addition of ClO^- (0–20 μM), a new absorption peak at around 720 nm increased dramatically, while the absorption signals at 556 nm decreased gradually. When ClO^- was added to 2 equivalents, the reaction basically completed, which was concomitant with a remarkable color change from purple to light green, as shown in Fig. 2 inset. Moreover, upon the addition of ClO^-, the emission peak at 520 nm decreased gradually, while a new sharp enhancement of the fluorescence emission at 600 nm ($\Phi_{1Free} < 0.1$, $\Phi_{1Hypochlorite} = 0.58$) and 820 nm ($\Phi_{2Free} < 0.1$, $\Phi_{2Hypochlorite} = 0.18$) was observed, as shown in Fig. 3. When ClO^- was added to 2 equivalents, the reaction was basically completed; the new emission peaks at 600 nm and 820 nm reached a maximum value. From the spectral property of **PDI-SY**, it could be

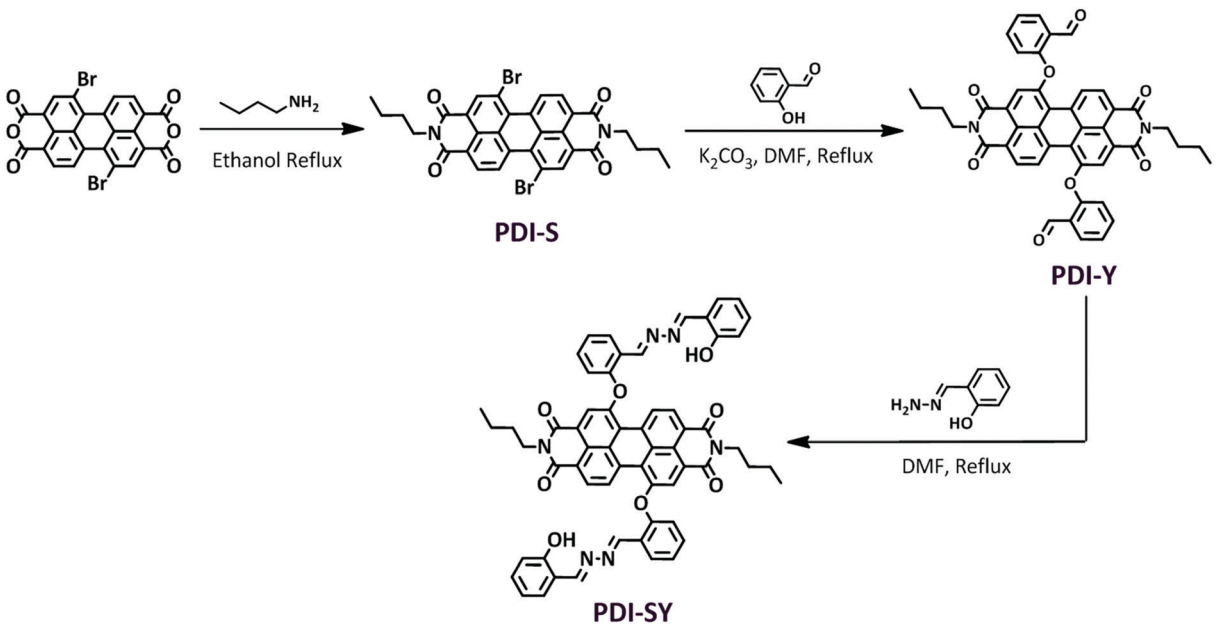

Scheme 1 Synthesis route of the probe **PDI-SY**.

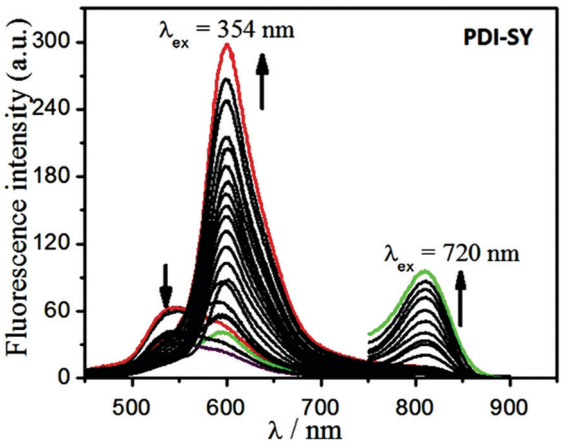

Fig. 3 Dual emission fluorescence spectra of **PDI-SY** as a function of the ClO^- concentration, ([**PDI-SY**] = 2 μM, λ_{ex} = 354 nm and 720 nm, V_{THF/H_2O} = 1 : 3, pH = 7.4, PBS buffer).

confirmed that **PDI-SY** can be used as a ratiometric fluorescent probe for sensing ClO^-.

Moreover, a linear relationship between the concentrations of ClO^- and the fluorescence intensity values of **PDI-SY** at 600 nm was observed (as shown in Fig. 3), the linear fitting curve of **PDI-SY** at 600 nm is shown in Fig. 4. According to this fitted equation, the detection limit of **PDI-SY** was measured to be 0.8×10^{-7} M (3σ/slope, σ is the standard deviation of the blank measurement). The above studies showed that **PDI-SY** can accurately and sensitively detect ClO^- (Table 1).

Rapid time responses of PDI-SY for ClO^- ions

The reaction rate of **PDI-SY** with the ClO^- ions is an important parameter to value its real-time tracking capability. As shown in Fig. 5, the reaction of **PDI-SY** with ClO^- can be triggered within 5 s without stirring, and completed in 60 s with a maximum emission intensity, indicating that **PDI-SY** can be employed as a rapid analytical chemosensor for the ClO^- detection. Simultaneously, the color of the solution containing **PDI-SY** changed from purple to light green gradually, as shown in Fig. 5 inset.

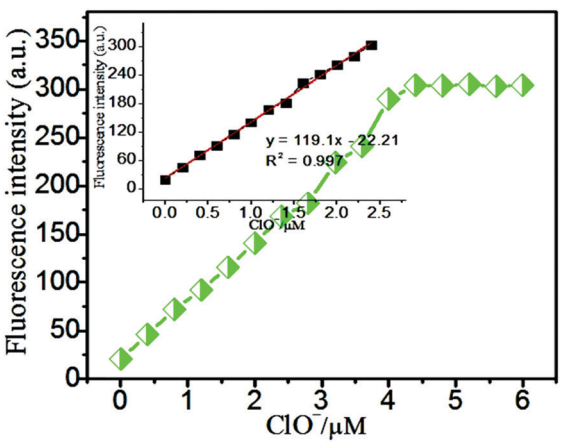

Fig. 4 Linear fitting curve of the probe **PDI-SY** with ClO^-, ([**PDI-SY**] = 2 μM, [ClO^-] = 2 equivalents, λ_{em} = 600 nm, V_{THF/H_2O} = 1 : 3).

Table 1 Fluorescence properties of **PDI-SY** in V_{THF/H_2O} = 1/3 at 298 K

Compounds	λ_{max}[a] (nm)	λ_{em}[b] (nm)	$\Delta\nu_1/\Delta\nu_2$[c] (cm^{-1})	Φ_1[d] at 600 nm	Φ_2[d] at 820 nm
PDI-SY	354/556	600	3947	<0.1	<0.1
PDI-SY-ClO^-	556/720	600/820	1692	0.58	0.18

[a] Absorption maximum. [b] Emission maximum. [c] Stoke's shift = $(1/\lambda_{abs} - 1/\lambda_{em}) \times 10^7$. [d] Fluorescence quantum yield, the fluorescence quantum yields were determined using rhodamine 6G and PDI (Φ = 0.95) as a standard, the max absorbance was used as the excited wavelength.[37]

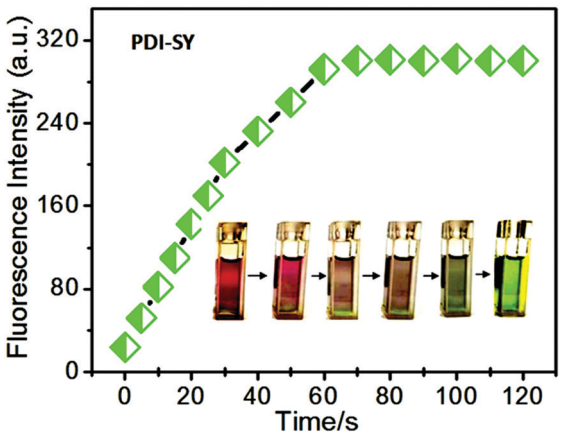

Fig. 5 Time-dependent fluorescence change of **PDI-SY** (2 μM) treated with ClO^-. λ_{ex} = 354 nm, λ_{em} = 600 nm, pH = 7.4, PBS buffer. (inset: photos of **PDI-SY** reacted with ClO^- ions in waste water from 5 seconds to 120 seconds).

The results demonstrate that **PDI-SY** has the ability for real-time monitoring of hypochlorite.

Selectivity and reversibility of PDI-SY to various ions

The interference experiments of the probe **PDI-SY** with other ions such as NO_2^-, *m*-Cl-ph-COOH, glutathione, cysteine, NO_3^-, PO_4^{3-} H_2O_2, Fe^{3+}, Ag^+, Ba^{2+}, Co^{2+}, Ni^{2+}, Cu^{2+}, Zn^{2+}, Cd^{3+}, Pb^{2+}, Mn^{2+} and Fe^{2+} were taken into account. First, eighteen parts of the **PDI-SY** solution with the same concentration were prepared. Then, the other ions were added to the solution, respectively. The fluorescence spectra of **PDI-SY** at 600 nm were collected. At last, ClO^- ions were added to the mixed solutions of **PDI-SY** with the other ions. All the fluorescence spectra excited at 354 nm were collected. As shown in Fig. 6, none of the other ions caused any fluorescence emission, while an obvious fluorescence enhancement occurred only after the addition of ClO^-, indicating that **PDI-SY** can detect ClO^- specifically.

PDI-SY shows good reversibility to ClO^- (as oxidant) and S^{2-} (as a reducing agent); the reversibility experiment was carried out by recording the emission intensity of **PDI-SY** at 600 nm with respect to the change of the ions ClO^-/S^{2-} up to 5 cycles. Fig. 7 shows the fluorescence intensity change of **PDI-SY** for 5 cycles. The relative standard deviations from five replicates were estimated to be <2%.

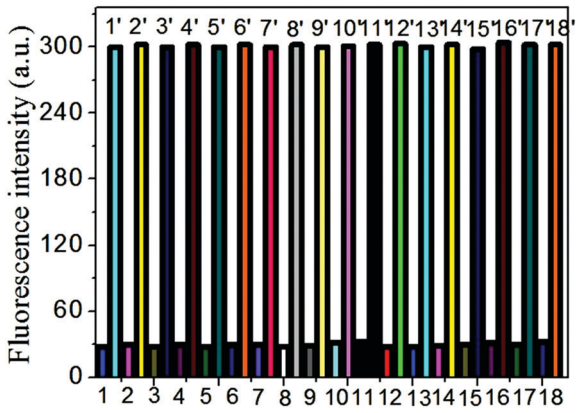

Fig. 6 Fluorescence spectra of the probe **PDI-SY** to numerous metal cations such as: (1–18) NO_2^-, *m*-Cl-ph-COOH, glutathione, cysteine, NO_3^-, PO_4^{3-} H_2O_2, Fe^{3+}, Ag^+, Ba^{2+}, Co^{2+}, Ni^{2+}, Cu^{2+}, Zn^{2+}, Cd^{3+}, Pb^{2+}, Mn^{2+} and Fe^{2+}, [**PDI-SY**] = 2 μM, λ_{ex} = 354 nm, λ_{em} = 600 nm, V_{THF/H_2O} = 1/3, pH = 7.4, PBS buffer.

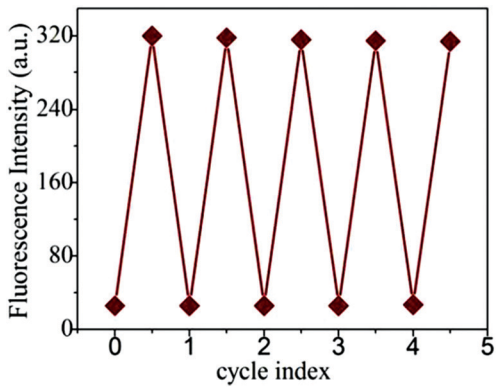

Fig. 7 Fluorescence intensity of **PDI-SY** at 600 nm ([**PDI-SY**] = 2 μM, λ_{ex} = 354 nm, in V_{THF/H_2O} = 1 : 3, pH = 7.4, PBS buffer) upon addition of ClO^- (2 equiv.) and S^{2-} solution up to 5 cycles.

PET and ICT-based mechanism discussion of PDI-SY with ClO^- ions

The possible mechanism of the **PDI-SY** reaction with the ClO^- ions is shown in Fig. 8, a PET process from the dibenzyliden–ehydrazine to the **PDI** core in the excited **PDI-SY** blocks the fluorescence emission of the **PDI** core. After the addition of the ClO^- ions, an oxidation reaction between **PDI-SY** and ClO^- ions occurred. The

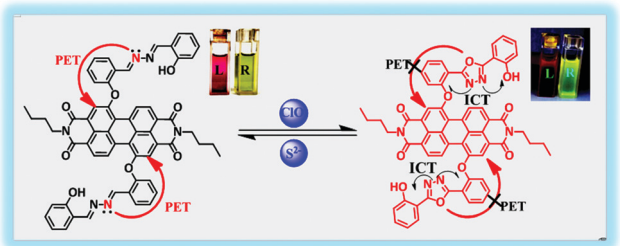

Fig. 8 The possible mechanism based on the PET and ICT of **PDI-SY** for detecting ClO^- ions.

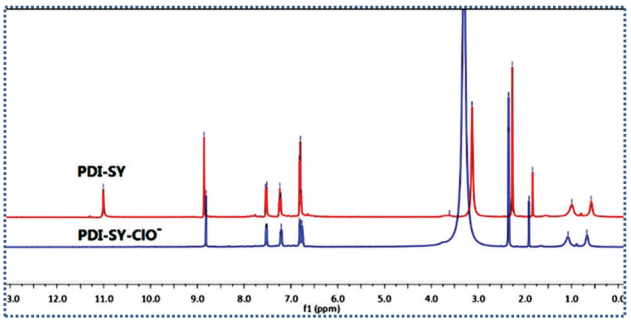

Fig. 9 ^{1}H NMR spectra of **PDI-SY** in the absence (top) and presence (bottom) of two equiv. of ClO^- in deuterated DMSO-d_6.

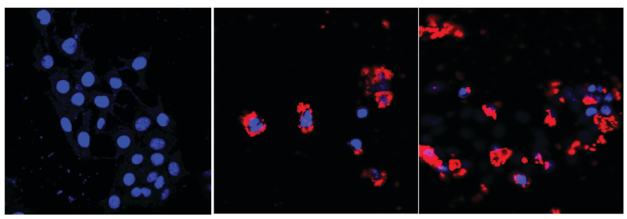

Fig. 10 Confocal laser scanning microscopy images of 4T1 cells incubated with **PDI-SY** (5 μM) for 30 min (left) and then further incubated with NaClO (10 μM) for 30 min (middle and right). Blue channel: λ_{ex} = 358 nm; red channel: λ_{ex} = 456 nm.

result of the oxidation reaction produces a new 1,3,4-oxadiazole ring that increases the conjugate plane of the new molecule, blocking the PET process in the probe, and producing the ICT process. Thus, the fluorescence of the probe recovered, and a new absorption peak at 720 nm appeared. Moreover, the reaction mechanism of **PDI-SY** with the ClO^- ions has been proved by ^{1}H NMR. As shown in Fig. 9, the ^{1}H NMR shifts of C═N–H in the probe is 11.0 ppm. However, after two equiv. of ClO^- was added, the peak at 11 ppm disappeared completely; simultaneously, no other new peak appeared. This change of ^{1}H NMR combined with the spectral property of **PDI-SY** strongly proves the possible mechanism of **PDI-SY** for the detection of ClO^- ions, as shown in Fig. 8. This discussion above is helpful for us to develop some new probes in the follow-up research work.

Confocal laser scanning microscopy images of PDI-SY with 4T1 cells

4T1 cells (≈10 000 cells per well) plated on a 96-well plate were cultured in fresh media that contained 10% fetal calf serum. **PDI-SY** at various concentrations was added and cultivated at 37 °C for 0.5 h. Then, 20 μl of NaClO (10 μM) was added to the well for 30 min. The CLSM imaging was performed on an Olympus FLUOVIEW FV1000 confocal laser scanning microscope. The cell nuclei were stained with DAPI (blue) and the cytoplasms were stained with NaClO modified **PDI-SY** (red), as shown in Fig. 10.

Conclusions

In summary, a near-infrared and ratiometric fluorescent probe **PDI-SY** designed on the PET and ICT mechanism, which

features a robust fluorescence ''light-up'' responses to ClO^- was successfully synthesized and **PDI-SY** was fully characterized by ^{1}H NMR, ^{13}C NMR, and high-resolution mass spectrometry. The probe can efficiently monitor ClO^- with rapid spectral responses within 5 s, low detection limit (0.8×10^{-7} M) and intense color changes (from purple to light green). In addition, **PDI-SY** can be used to detect the hypochlorite for 5 cycles, the new detection mechanism of **PDI-SY** for ClO^- ions was proved by ^{1}H NMR for the first time. More importantly, the application of ClO^- detection in cell imaging has also been achieved. Therefore, we expect that **PDI-SY** may provide a new strategy for the detection of ClO^- in biological application.

Experimental

Materials and methods

^{1}H NMR and ^{13}C NMR spectra were recorded on a Bruker ADVANCE 300 NMR spectrometer in $CDCl_3$ or DMSO. HRMS were recorded on an Ultraflex II MALDI-TOF mass spectrometer. UV-visible absorption spectra were recorded on a Shimadu UV-3600 spectrophotometer. Fluorescence spectra were recorded on a HORIBA FL-4 Max spectrometer. FT-IR spectra were recorded on a Nicolet 750 series in the region of 4000–400 cm^{-1}. The CLSM imaging was performed on Olympus FLUOVIEW FV1000 confocal laser scanning microscope. All the reagents used were purchased from Aladdin. The solvent used in the test was PBS buffer.

Synthesis

Compound 2-(hydrazonomethyl)phenol was prepared our laboratory according to the modified published methods.[38] The structure of the compounds **PDI-S**, **PDI-Y** and the compound **PDI-SY** was characterized by ^{1}H NMR and their spectra have been displayed in the ESI.†

Compound PDI-S. Compound 1,7-bis(4-*tert*-butylphenyloxy)-perylene-3,4:9,10-tetracar-boxylic acid bisanhydride (4.0 g, 7.3 mmol), and *n*-butylamine (0.53 g, 1.5 mmol) was dissolved in ethanol (80 ml), the mixture was heated under reflux for 12 h. After cooled to room temperature, the solvent was removed under reduced pressure, a red-black solid was observed, which was washed with water (100 ml) and dried in 60 °C. It was used for the next reaction without further purification. ^{1}H NMR (DMSO, ppm): δ 8.67–8.65 (d, 3H, J = 6 Hz), 8.46–8.44 (d, 3H, J = 6 Hz), 4.15–4.10 (m, 4H), 1.96–1.95 (m, 2H), 1.41–1.23 (m, 6H), 0.97–0.90 (m, 6H).

Compound PDI-Y. In N_2 atmosphere, compound **PDI-S** (3.0 g, 4.5 mmol), *o*-hydroxybenzaldehyde (1.1 g, 9 mmol), K_2CO_3 (1.5 g, 15 mmol), and DMF (40 ml) were mixed and the mixture was heated at 100 °C for 8 h. After cooled to the room temperature, water (40 ml) was added and the pH value was adjusted to weak acidic using 1N hydrochloric acid resulting in the precipitation of black solid. Subsequently it was dried in a vacuum drying oven at 50 °C for 24 hours, to give a yellow solid 3.2 g, yield: 95%. It was used for the next reaction without further purification. ^{1}H NMR (DMSO, ppm): δ 10.25 (s, 2H), 8.99 (s, 4H), 7.99–7.94 (m, 2H), 7.64–7.52 (m, 3H), 7.49–7.25 (m, 3H), 6.97–6.94 (m, 6H), 4.15–4.10 (m, 4H), 1.98–1.96 (m, 2H), 1.41–1.23 (m, 6H), 0.97–0.90 (m, 6H). TOF-MS-ES: *m*/*z*. Calculated: $[M + H]^+$ = 743.238, found: $[M + H]^+$ = 743.236.

Compound PDI-SY. Compound **PDI-Y** (2.0 g, 2.7 mmol), compound salicylhydrazine (5.9 mmol excess), and DMF (60 ml) was mixed, the mixture was heated at 80 °C for 12 h. After cooled to room temperature, water (60 ml) was added resulting in the precipitation of a black solid which was filtrated and dried in a blast drying oven at 60 °C. Then, it was purified *via* recrystallization by ethanol to give a black solid 2.9 g, yield: 92%. FT-IR (KBr) cm^{-1}: 3452 (νC═C–H); 2932–2980 (νC–H); 1602 (ν_{as}H–C═C) 1498 (ν_s–C═C) 1276 (νC–O).^{1}H NMR (DMSO, ppm): δ 11.12 (s, 4H), 8.99 (s, 4H), 7.68 (m, 5H), 7.42–7.38 (t, 5H, J = 6 Hz), 6.99–6.95 (m, 10H), 3.86–3.80 (m, 4H), 2.07 (m, 2H), 1.25 (m, 6H), 0.88 (m, 6H). ^{13}C NMR (DMSO, ppm): δ 192.17, 162.78, 161.20, 136.89, 129.65, 122.76, 117.69, 36.25, 31.24, 22.97, 14.39. TOF-MS-ES: *m*/*z*. Calculated: $[M + H]^+$ = 979.3450, found: $[M + H]^+$ = 979.3450.

Conflicts of interest

There are no conflicts to declare.

Acknowledgements

This work was supported by PhD Botao Qu for confocal laser scanning cell images, the''Qinglan project'' of Jiangsu Province (2018–2012) College of Chemistry and Chemical Engineering, Yangzhou Polytechnic Institute, the Fundamental Research Funds for the National Natural Science Foundation of China (No. 51372077), and the Natural Science Foundation of Shanxi Province (No. 201901D111213).

References

1 Y. Y. Zhang, Y. F. Ma, Z. Wang, X. Y. Zhang, X. Chen and H. M. Wang, *Analyst*, 2020, **145**, 939–945.
2 X. J. He, C. C. Xu, W. Xiong, Y. Qian, J. Y. Fan, F. Ding, H. Deng, H. Chen and J. L. Shen, *Analyst*, 2020, **145**, 29–33.
3 Y. P. Pan, Y. Yan, Y. Li, X. W. Gao and D. B. Chao, *New J. Chem.*, 2019, **43**, 15120–15125.
4 S. Malkondu, S. Erdemir and S. Karakurt, *Dyes Pigm.*, 2020, **174**, 108019.
5 X. P. Lin, Y. L. Chen, L. Bao, S. J. Wang, K. Y. Liu, W. D. Qin and F. G. Kong, *Dyes Pigm.*, 2020, **174**, 108113.
6 G. C. Bittner, C. R. Bertozzi and C. J. Chang, *J. Am. Chem. Soc.*, 2013, **135**, 1783–1795.
7 K. B. Li, L. Dong, S. Zhang, W. Shi, W. P. Jia and D. M. Han, *Talanta*, 2017, **165**, 593–597.
8 N. Güngör, A. M. Knaapen, A. Munnia, M. Peluso, G. R. Haenen, R. K. Chiu, R. W. L. Godschalk and F. J. Van Schooten, *Mutagenesis*, 2010, **25**, 149–154.
9 Y. C. Du, B. W. Wang, D. Jin, M. R. Li, Y. Li, X. L. Yan, X. Q. Zhou and L. G. Chen, *Anal. Chim. Acta*, 2019, **12**, 23.

10 C. P. Jiao, Y. Y. Liu, W. J. Lu, P. P. Zhang, X. Ma and Y. F. Wang, *RSC Adv.*, 2019, **9**, 31196–31201.
11 M. R. Li, F. K. Du, P. Xue, X. C. Tan, S. G. Liu, Y. Zhou, J. Chen and L. J. Bai, *Spectrochim. Acta, Part A*, 2020, **227**, 117760.
12 J. Lv, F. Wang, T. W. Wei and X. Q. Chen, *Ind. Eng. Chem. Res.*, 2017, **56**, 3757–3764.
13 W. J. Shi, Y. Huang, W. C. Liu, D. Xu, S. T. Chen, F. G. Liu, J. Q. Hu, L. Y. Zheng and K. Chen, *Dyes Pigm.*, 2019, **170**, 107566.
14 X. H. Xu, C. Liu, Y. Mei and Q. H. Song, *J. Mater. Chem. B*, 2019, **7**, 6861–6867.
15 X. L. Zhong, Q. Yang, Y. S. Chen, Y. L. Jiang, B. X. Wang and J. Shen, *J. Mater. Chem. B*, 2019, **7**, 7332–7337.
16 J. S. Lan, L. Liu, R. F. Zeng, Y. H. Qin, Y. Liu, X. Y. Jiang, A. Aihemaiti, Y. Ding, T. Zhang and R. J. Y. Hoc, *Chem. Commun.*, 2020, **56**, 1219–1222.
17 G. J. Mao, G. Q. Gao, Z. Z. Liang, Y. Y. Wang, L. Su, Z. X. Wang, H. Zhang, Q. J. Ma and G. S. Zhang, *Anal. Chim. Acta*, 2019, **1081**, 184–192.
18 M. Ren, Z. H. Li, J. Nie, L. Wang and W. Y. Lin, *Chem. Commun.*, 2018, **54**, 9238–9241.
19 D. Wu, L. Y. Chen, Q. L. Xu, X. Q. Chen and J. Y. Yoon, *Acc. Chem. Res.*, 2019, **52**, 2158–2168.
20 Y. L. Pak, S. J. Park, Q. L. Xu, H. Myung Kim and J. Yoon, *Anal. Chem.*, 2018, **90**, 9510–9514.
21 L. Wang, X. L. Chen, Q. Xia, R. Y. Liu and J. Q. Qu, *Ind. Eng. Chem. Res.*, 2018, **57**, 7735–7741.
22 Y. V. Zatsikha, N. O. Didukh, R. K. Swedin, V. P. Yakubovskyi, T. S. Blesener, A. T. Healy, D. E. Herbert, D. A. Blank, V. N. Nemykin and Y. P. Kovtun, *Org. Lett.*, 2019, **21**, 5713–5718.
23 B. L. Huo, M. Du, A. Shen, M. W. Li, Y. R. Lai, X. Bai, A. J. Gong, L. Q. Fang and Y. X. Yang, *Sens. Actuators, B*, 2019, **284**, 23–29.
24 Y. L. Zhu, K. N. Wang, X. W. Wu, Y. N. Sun, X. S. Gong, D. X. Cao, R. F. Guan and Z. Q. Liu, *Talanta*, 2020, **209**, 120548.
25 Y. F. Huang, Y. B. Zhangb, F. J. Huob, J. B. Chaob and C. Yin, *Sens. Actuators, B*, 2019, **287**, 453–458.
26 Y. L. Wu, J. Wang, F. Zeng, S. L. Huang, J. Huang, H. T. Xie, C. M. Yu and S. Z. Wu, *ACS Appl. Mater. Interfaces*, 2016, **8**(2), 1511–1519.
27 C. DuanMiae, W. VerwilstJunchao, X. Seok, K. Zeng and J. S. Kim, *Anal. Chem.*, 2019, **91**(6), 4172–4178.
28 X. M. Zou, X. B. Zhou, C. Cao, W. Y. Lu, W. Yuan, Q. Y. Liu, W. Feng and F. Y. Li, *Nanoscale*, 2019, **11**, 2959–2965.
29 C. Xu, Y. Qian, Z. Q. Qi, C. G. Lu and Y. P. Cui, *New J. Chem.*, 2018, **42**, 6910–6917.
30 Y. Y. Zhang, Y. F. Ma, Z. Wang, X. Y. Zhang, X. Chen, S. C. Hou and H. M. Wang, *Analyst*, 2020, **145**, 939–945.
31 H. B. Gobeze, L. M. Arellano, A. M. Gutiérrez-Vílchez, M. J. Gómez-Escalonilla, Á. Sastre-Santos, F. Fernández-Lázaro, F. Lang and F. D'Souz, *Nanoscale Adv.*, 2019, **1**, 4009–4015.
32 W. Zhang, Y. Song, S. J. He, L. Shang, R. N. Ma, L. P. Jia and H. S. Wang, *Nanoscale*, 2019, **11**, 20910–20916.
33 Y. X. Zhou, B. Xue, C. Y. Wu, S. Q. Chen, H. Liu, T. G. Jiu, Z. B. Li and Y. J. Zhao, *Chem. Commun.*, 2019, **55**, 13570–13573.
34 M. Li, J. Xu, W. F. Guo, W. C. Zhong, Q. Li, L. L. Tan and L. Shang, *Sens. Actuators, B*, 2020, **305**, 127422.
35 P. Singh, L. S. Mittal, K. Kumar, P. Sharma, G. Bhargava and S. Kumara, *Chem. Commun.*, 2018, **54**, 9482–9485.
36 K. Kumar, S. Kaur, S. Kaur, G. Bhargava, S. Kumar and P. Singh, *J. Mater. Chem. B*, 2020, **8**, 125–135.
37 J. N. Demas and G. A. Crosby, *J. Phys. Chem.*, 1971, **75**, 991–1024.
38 B. Gregory, L, N. Donna M and J. Branko S, *Bioorg. Med. Chem.*, 2014, **22**(17), 4629–4636.